Proton-nucleus elastic scattering: Comparison between phenomenological and microscopic optical potentials

Matteo Vorabbi,[1] Paolo Finelli,[2] and Carlotta Giusti[3]
[1]*TRIUMF, 4004 Wesbrook Mall, Vancouver, British Columbia, Canada V6T 2A3*
[2]*Dipartimento di Fisica e Astronomia, Università degli Studi di Bologna and INFN, Sezione di Bologna, Via Irnerio 46, I-40126 Bologna, Italy*
[3]*Dipartimento di Fisica, Università degli Studi di Pavia and INFN, Sezione di Pavia, Via A. Bassi 6, I-27100 Pavia, Italy*

(Received 5 June 2018; published 4 December 2018)

Background: Elastic scattering is a very important process to understand nuclear interactions in finite nuclei. Despite decades of efforts, the goal of reaching a coherent description of this physical process in terms of microscopic forces is still far from being completed.
Purpose: In previous papers we derived a nonrelativistic theoretical optical potential from nucleon-nucleon chiral potentials at fourth (N^3LO) and fifth order (N^4LO). We checked convergence patterns and established theoretical error bands. With this work we study the performances of our optical potential in comparison with those of a successful nonrelativistic phenomenological optical potential in the description of elastic proton scattering data on several isotopic chains at energies around and above 200 MeV.
Methods: We use the same framework and the same approximations as adopted in our previous papers, where the nonrelativistic optical potential is derived at the first-order term within the spectator expansion of the multiple scattering theory and adopting the impulse approximation and the optimum factorization approximation.
Results: The cross sections and analyzing powers for elastic proton scattering off calcium, nickel, tin, and lead isotopes are presented for several incident proton energies, exploring the range $156 \leqslant E \leqslant 333$ MeV, where experimental data are available. In addition, we provide theoretical predictions for ^{56}Ni at 400 MeV, which is of interest for the future experiments at EXL.
Conclusions: Our results indicate that microscopic optical potentials derived from nucleon-nucleon chiral potentials at N^4LO can provide reliable predictions for the cross section and the analyzing power both of stable and exotic nuclei, even at energies where the reliability of the chiral expansion starts to be questionable.

DOI: 10.1103/PhysRevC.98.064602

I. INTRODUCTION

The scattering process of an incident nucleon off a target nucleus is a widespread experimental tool for investigating, with specific nuclear reactions, the different properties of a nuclear system. Elastic scattering is probably the main event occurring in the nucleon-nucleus (NA) scattering and measurements of cross sections and polarization observables in elastic proton-nucleus (pA) scattering have provided a lot of detailed information on nuclear properties [1,2].

A huge amount of experimental data has been collected over the last years concerning stable nuclei (usually with proton or neutron numbers corresponding to some magic configurations), but nowadays one of the most active areas of research in nuclear physics is to understand the properties of nuclei far from the beta-stability line. A number of radioactive ion-beam facilities will be used in next years for this purpose. In particular, we would like to mention the FAIR project, with the section dedicated to electromagnetic and light hadronic probes (EXL) [3,4], where the structure of unstable exotic nuclei in light-ion scattering experiments at intermediate energies will be extensively studied. Some preliminary measurements have already been performed by investigating the reaction ^{56}Ni$(p, p)^{56}$Ni at an energy of 400 MeV/u in inverse kinematics [5]. The authors of Ref. [5] claim that the preliminary results are very promising and demonstrate the feasibility of the intended program of EXL. This result strongly supports the need of a reliable description of the interaction of a nucleon with stable and unstable nuclei. Unfortunately, such processes are characterized by many-body effects that make their theoretical description an extremely hard task.

A very useful framework to achieve this goal is provided by the theoretical concept of the optical potential (OP), where the complicated nature of the NA interaction is described introducing a complex effective potential whose real part describes the average interaction between the projectile and the target, and the imaginary part describes the effect of all inelastic processes which tend to deplete the flux in the elastic channel [6]. The OP was originally employed to analyze the NA elastic-scattering data, but its use has been afterwards extended to inelastic scattering and to a wide variety of nuclear reactions.

Different OPs for elastic NA scattering have been derived either by phenomenological analyses of experimental data or by a more fundamental microscopic calculation. Phenomenological OPs are obtained assuming an analytical form of the potential which depends on some free parameters

specifying the well and the geometry of the system and that are determined by a fitting procedure over a set of available experimental data of elastic pA scattering. This approach provides good OPs, which perform very well in many regions of the nuclear chart and for several energy ranges where data are available, but which may lack predictive power when applied to situations where experimental data are not yet available. Instead, microscopic OPs are derived by starting from the nucleon-nucleon (NN) interaction; they can be obtained by using different NN potentials and different methods depending on the mass of the target and on the energy of the reaction of interest, and do not contain free adjustable parameters. A recent list of the different approaches can be found in Ref. [7]. Being the result of a model and not of a fitting procedure, microscopic OPs should have more theoretical content and might have a more general predictive power than phenomenological OPs, but the approximations which are needed to reduce the complexity of the original many-body problem, whose exact solution is for complex nuclei beyond our present capabilities, might give a poorer agreement with available empirical data.

In Ref. [8] we constructed a microscopic OP for elastic pA scattering starting from NN chiral potentials derived up to N^{3}LO in the chiral expansion and we studied the chiral convergence of the NN potential in reproducing the pA scattering observables. The OP was obtained at the first-order term within the spectator expansion of the nonrelativistic multiple scattering theory and adopting the impulse approximation and the optimum factorization approximation. In a subsequent work [9] we adopted the same model to obtain the OP and we studied the chiral convergence of a new generation of NN chiral interactions derived up to N^{4}LO. Our conclusion was that the convergence has been reached at N^{4}LO.

In this work we perform a systematic investigation of the predictive power of our microscopic OP derived in Ref. [9] from different chiral potentials at N^{4}LO and of the successful phenomenological OP of Refs. [10,11] in comparison with available data for the observables of elastic proton scattering on different isotopic chains, located in different areas of the nuclear chart. Results are presented for several proton energies around and above 200 MeV, with the aim to test the upper energy limit of applicability of our OP before the chiral expansion scheme breaks down.

The paper is organized as follows: In Sec. II we summarize the main features of both microscopic and phenomenological approaches to the OP. In Sec. III we show and discuss the results for the observables of elastic pA scattering. Finally, in Sec. IV we draw our conclusions.

II. THEORETICAL MODELS

The underlying assumption on which the OP is based is that the interaction between the projectile and the target nucleus can be modelled by a complex mean-field potential. The numerical solution of the Schrödinger equation (or the Lippmann–Schwinger equation in the momentum space representation) with this complex potential brings valuable information, i.e., the differential cross section $d\sigma/d\Omega$, the analyzing power A_y, and the spin rotation Q among others [1,2].

In our approach we limit ourselves to the study of the elastic channel, which is defined as the case in which the target and the projectile remain in the stationary state, at energies where a nonrelativistic description can be conveniently applied. Given a state $|\mathbf{k}^{\dagger}_{el}\rangle$ which describes the relative motion of both collision partners, after some manipulations, a Schrödinger equation can be derived for the projectile and the target in the relative motion that reads as follows:

$$(T + V_{\rm opt} - E)|\mathbf{k}^{\dagger}_{el}\rangle = 0. \tag{1}$$

T is the kinetic-energy operator, E is the available energy in the elastic channel, and $V_{\rm opt}$ is the so-called generalized OP [6] defined as

$$V_{\rm opt} = V_{2b} + V_{2b}\,Q\,\frac{1}{E - QHQ + i\eta}\,QV_{2b}, \tag{2}$$

where V_{2b} is a two-body potential, and P and Q are idempotent projection operators introduced to isolate the contribution of the elastic channel: P projects onto the elastic channel and Q onto the complementary space, i.e., onto all the nonelastic channels, for which the following relations hold: $Q = 1 - P$ and $QP = PQ = 0$.

The first term in Eq. (2) is the contribution of the static two-body interaction, while the second term takes into account the effect of nonelastic channels in the space Q. This term is the dynamic part of the OP and depends on the energy of the elastic channel. As a consequence, the Feshbach approach naturally leads to an energy-dependent OP $V_{\rm opt}(E)$.

The general structure of $V_{\rm opt}$ is extremely complicated and can be simplified for some specific applications. We refer the reader to Refs. [1,2,12,13] for exhaustive discussions about the approximations which are necessary to deal with the treatment of $V_{\rm opt}$. Here we will restrict our considerations to the bare essentials.

Generally speaking, there are two available methods for the construction of an OP.

In the microscopic approach, one starts from a realistic NN interaction (i.e., able to reproduce the experimental NN phase shifts with a χ^2 per datum very close to one [14–16]) and an educated guess for the radial density of the target [1,2,12]. A suitable combination of these two terms (a procedure usually called "folding") produces the optical potential $V_{\rm opt}$. The main features of the microscopic OP are the independence from phenomenological inputs and, in particular with the most recent NN microscopic potentials, the ability to assess reliable error estimates (see Ref. [17] for extensive discussions about this topic). In the ideal case where no approximations are made to derive the microscopic OP, the absence of phenomenology would lead to accurate predictions that are probably better than those obtained with a phenomenological OP, but in practice the full calculation of the OP turns out to be too complicated and the approximations that must necessarily be introduced reduce the accuracy and the reliability of these predictions.

On the other hand, a more pragmatic phenomenological approach can be pursued with the adoption of an analytical form of the potential, i.e., like a Woods–Saxon shape, where the

adjustable parameters are fit to a set of available experimental data [18].

Since a lot of efforts has been put over the last years on both methods, we believe that it can be useful to make a comparison between the above-mentioned approaches. For this purpose, we decided to use our recent microscopic OPs derived [9] from NN chiral interactions at N^{4}LO [17,19–21] and the most recent analysis by Koning *et al.* [10] who developed a very successful nonrelativistic phenomenological OP (KD) for energies below 200 MeV but also with an extension up to 1 GeV [11].

A. Microscopic optical potentials at N^{4}LO

The theoretical justification for the description of the NA optical potential in terms of the microscopical NN interaction has been addressed for the first time by Watson *et al.* [22] and then formalized by Kerman *et al.* (KMT) [23], where the so-called multiple-scattering approach to the NA optical potential is expressed by a series expansion of the free NN scattering amplitudes. Over the last decades several authors made important contributions to this approach. Just to mention the most relevant ones, we would like to recall the works with the KMT optimum factorized OP [24,25], the calculation of the full-folding OP with harmonic-oscillator densities [26–29], the calculation of the second-order OP in the multiple scattering theory [30], the calculation of the medium contributions to the first-order OP [31–33], and the calculation of the full-folding OP with realistic densities [34]. Concerning the inclusion of medium effects we also want to mention the works based on the g matrix of Amos *et al.* [35] and Arellano *et al.* [36,37].

In Refs. [8,9] a microscopic OP was obtained at the first-order term within the spectator expansion of the nonrelativistic multiple-scattering theory, corresponding to the single-scattering approximation. The impulse approximation was adopted, where nuclear binding forces on the interacting target nucleon are neglected, as well as the optimum factorization approximation, where the two basic ingredients of the calculations, i.e., the nuclear density and the NN t matrix, are factorized. We refer the reader to Refs. [8,9] for all relevant details and an exhaustive bibliography. In momentum space, the factorized $V_{\rm opt}$ is obtained as

$$V_{\rm opt}(\mathbf{q},\mathbf{K};\omega) \sim \sum_{N=n,p} t_{pN}\left[\mathbf{q},\frac{A+1}{A}\mathbf{K};\omega\right]\rho_N(q), \qquad (3)$$

where t_{pN} represents the proton-proton (pp) and proton-neutron (pn) free t matrix evaluated at a fixed energy ω, ρ_N is the neutron and proton profile density, and the incoming and outgoing projectile momenta $\mathbf{k}$ and $\mathbf{k}'$ are conveniently expressed by the variables $\mathbf{q}\equiv\mathbf{k}'-\mathbf{k}$ and $\mathbf{K}\equiv\frac{1}{2}(\mathbf{k}'+\mathbf{k})$ (see Sec. II of Ref. [8]).

For the neutron and proton densities of the target nucleus we use as in Refs. [8,9] a relativistic mean-field (RMF) description [38], which has been quite successful in the description of the ground-state and excited-state properties of finite nuclei, in particular in a density dependent meson exchange (DDME) version, where the couplings between mesonic and baryonic fields are assumed as functions of the density itself [39]. We are aware that a phenomenological description of the target is not fully consistent with the goal of a microscopic description of elastic NA scattering. In a very recent paper [40] a microscopic OP was derived by using *ab initio* translationally invariant nonlocal one-body nuclear densities computed within the no-core shell-model (NCSM) approach [41], which is a technique particularly well suited for the description of light nuclei. Indeed, the use of a nonlocal *ab initio* density improves significantly the agreement with data of elastic proton scattering off ^{4}He and ^{12}C, while for ^{16}O no significant improvement is obtained in comparison with the RMF results. The work reported in Ref. [40] represents a great leap forward towards the construction of a microscopic OP for light nuclei, but the aim of our present work is to investigate the predictive power of a microscopic OP over a wide range of nuclei and isotopic chains in different regions of the nuclear chart.

For the NN interaction we use here two different versions of the chiral potentials at fifth order (N^{4}LO) recently derived by Epelbaum, Krebs, and Meißner (EKM) [17,19] and Entem, Machleidt, and Nosyk (EMN) [20,21]. As explained in Ref. [9], the two versions of the chiral N^{4}LO potentials have significant differences concerning the renormalization procedures and we follow the same prescriptions adopted there. The strategy followed for the EKM potentials [17,19] consists of a coordinate space regularization for the long-range contributions $V_{\rm long}(\boldsymbol{r})$ by the introduction of $f(\frac{r}{R}) = [1-\exp(-\frac{r^2}{R^2})]^n$, and a conventional momentum-space regularization for the contact (short-range) terms, with a cutoff $\Lambda = 2R^{-1}$. Five choices of R are available: 0.8, 0.9, 1.0, 1.1, and 1.2 fm, leading to five different potentials.

On the other hand, for the EMN potentials, a slightly more conventional approach was pursued [20,21]. A spectral function regularization, with a cutoff $\tilde{\Lambda} \simeq 700$ MeV, was employed to regularize the loop contributions and a conventional regulator function, with $\Lambda = 450$, 500, and 550 MeV, to deal with divergences in the Lippmann–Schwinger equation. For all details we refer the reader to Refs. [9,20,21].

The aim of the present work is to test the predictive power of our microscopic OP in comparison with available experimental data and it can be useful to show the uncertainties on the predictions produced by NN chiral potentials obtained with different values of the regularization parameters. For this purpose, all calculations have been performed with three of the EKM [17,19] potentials, corresponding to $R = 0.8$, 0.9, and 1.0 fm, and with two of the EMN [20,21] potentials, corresponding to $\Lambda = 500$ and 550 MeV. In all the figures presented in Sec. III, the bands give the differences produced by changing R for EKM (red bands) and Λ for EMN (green bands). Thus the bands have here a different meaning than in Ref. [9], where the EKM and EMN NN chiral potentials at N^{4}LO were also used. The aim of Ref. [9] was to investigate the convergence and to assess the theoretical errors associated with the truncation of the chiral expansion and the bands were given to investigate these issues. We also showed in Ref. [9] that EKM calculations based on different values of R are quite close and consistent with each other (although, as remarked in Ref. [19], larger values of R are probably less accurate due to a larger influence of cutoff artifacts). The same assumption can be made about the EMN potentials: changing the cutoffs does

not lead to sizable differences in the χ^2/datum (see Table VIII in Ref. [21]) and it is safe to perform calculations with only two potentials. Because we want to explore elastic scattering at energies around and above 200 MeV, we exclude the EKM potentials with $R = 1.1$ and 1.2 fm and the EMN potential with $\Lambda = 450$ MeV. We are confident that for our present purposes showing results with only a limited set of NN chiral potentials will not affect our conclusions in any way.

B. Phenomenological potentials

One of the most recent and successful phenomenological OPs was developed by Koning *et al.* [10]. As quoted in the original paper, the authors provided a phenomenological OP able to challenge the best microscopic approaches in terms of predictive power.

The phenomenological OP $V_{\rm opt}$ for proton-nucleus scattering is usually defined as [10]

$$V_{\rm opt} = -V_V(r,E) - iW_V(r,E) - iW_D(r,E) + V_{SO}(r,E)\mathbf{l}\cdot\mathbf{s} + iW_{SO}(r,E)\mathbf{l}\cdot\mathbf{s} + V_C(r,E), \quad (4)$$

where $V_{V,SO}$ and $W_{V,D,SO}$ are the real and imaginary components of the volume-central (V), surface-central (D), and spin-orbit (SO) potentials, respectively, and E is the laboratory energy of the incident particle. All the components are separated in energy-dependent well depths and energy-independent shape functions as $V(r,E) \sim \tilde{V}(E)f(r)$ and $W(r,E) \sim \tilde{W}(E)f(r)$, where the radial functions usually resemble a Woods–Saxon shape (in the volume case) and the radial derivative of a Woods–Saxon shape (in the other cases). The Coulomb term V_C is usually given by that of a uniformly charge sphere.

The potential of Ref. [10] is a so-called "global" OP, which means that the free adjustable parameters are fit for a wide range of nuclei ($24 \leqslant A \leqslant 249$) and of incident energies (1 keV $\leqslant E \leqslant$ 200 MeV) with some parametric dependence of the coefficients in terms of the target mass number A and of the incident energy E. An alternative choice, not adopted in Ref. [10], would be to produce an OP for each single target nucleus. We refer the reader to Ref. [10] for more details. Recently, an extension of the OP of Ref. [10] up to 1 GeV has been proposed [11]. It is generally believed that above ∼180 MeV the Schrödinger picture of the phenomenological OP should be taken over by a Dirac approach [42], but the extension was done just with the aim to test at which energy the validity of the predictions of the nonrelativistic OP fails. We are aware that above 200 MeV an approach based on the Dirac equation would probably be a more consistent choice, but since we are interested in testing the limit of applicability of our (nonrelativistic) microscopic OP we will use such an extension to perform some benchmark calculations at center-of-mass energies close to 300 MeV. All the calculations have been performed by ECIS-06 [43] as a subroutine in the TALYS software [42,44].

III. RESULTS

The aim of the present paper is to investigate and compare the predictive power of our microscopic OP derived from the EKM [17,19] and EMN [20,21] chiral potentials at N^{4}LO and of the phenomenological global OP KD derived by Koning *et al.* [10,11] in comparison with available data of elastic pA scattering. To this aim, in this section we present and discuss the predictions of the different OPs for the differential cross section $\frac{d\sigma}{d\Omega}$, presented as a ratio to the Rutherford cross section, $\frac{d\sigma}{d\Omega}/\frac{d\sigma}{d\Omega}_{\rm Ruth}$, and analyzing power A_y of proton elastic scattering over a wide range of nuclei and isotope chains, from oxygen to lead, and for proton energies between 156 and 333 MeV, for which experimental data are available.

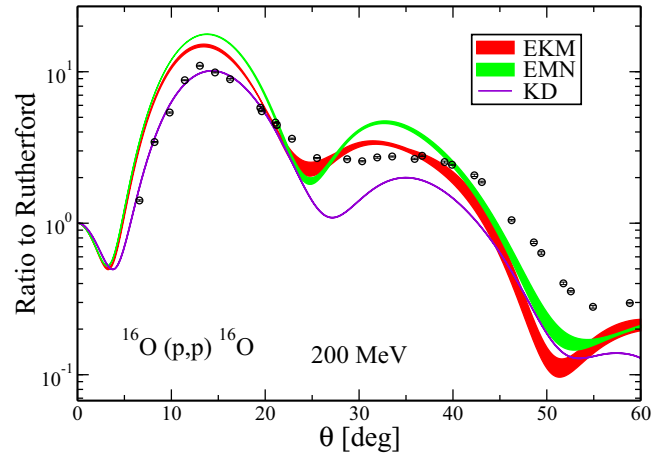

FIG. 1. Ratio of the differential cross section to the Rutherford cross section as a function of the center-of-mass scattering angle θ for elastic proton scattering off ^{16}O. Calculations are performed at $E = 200$ MeV (laboratory energy) with the microscopic OPs derived from the EKM [17,19] (EKM, red band) and EMN [20,21] (EMN, green band) NN chiral potentials at N^{4}LO and with the phenomenological global OP of Ref. [42] (KD, violet line). The interpretation of the bands is explained in the text. Experimental data are from Refs. [45,46].

The energy range considered for our investigation was chosen on the basis of the assumptions and approximations adopted in the derivation of the theoretical OP. In particular, the impulse approximation does not allow us to use our microscopic OP with enough confidence at much lower energies, where we can expect that the phenomenological KD potential is able to give a better agreement with the experimental data. The upper energy limit is determined by the fact that the EKM and EMN chiral potentials are able to describe NN scattering observables up to 300 MeV [17,19–21]. The phenomenological global KD potential was originally constructed for energies up to 200 MeV [10] and it was then extended up to 1 GeV [11]. It can therefore be interesting to test and compare the validity of the predictions of both microscopic and phenomenological OPs up to about 300 MeV.

In Ref. [9] we compared the results obtained with different versions of EKM and EMN chiral potentials at N^{4}LO for the pp and pn Wolfenstein amplitudes and for the scattering observables of elastic proton scattering off ^{12}C, ^{16}O, and ^{40}Ca nuclei at an incident proton energy $E = 200$ MeV. For the sake of comparison with our previous work, we show in Fig. 1 the ratio of the differential cross section to the

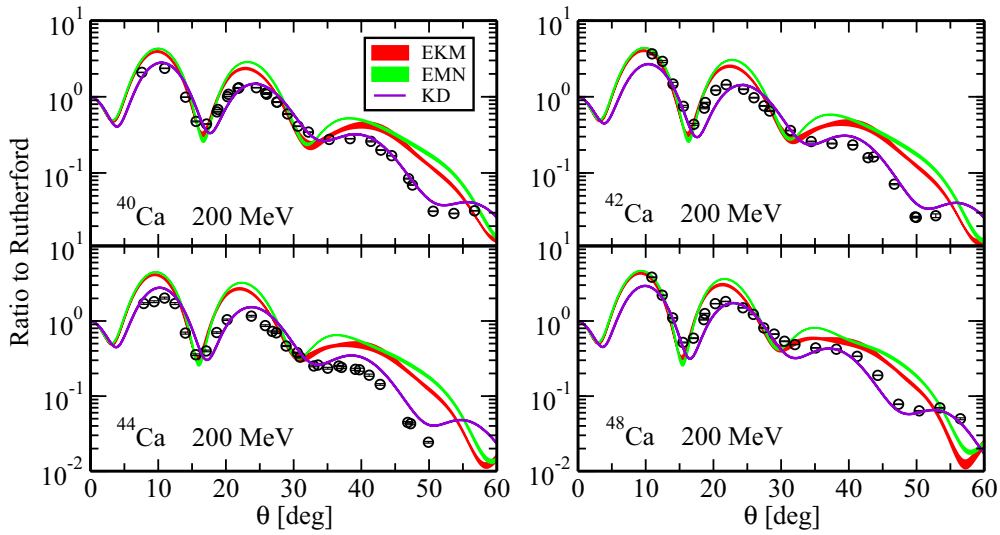

FIG. 2. The same as in Fig. 1 for ^{40,42,44,48}Ca isotopes at 200 MeV. Experimental data are from Refs. [45,46].

Rutherford cross section for elastic proton scattering off ^{16}O at $E = 200$ MeV. The results obtained with the EKM and EMN potentials and with the KD optical potential are compared with the experimental data taken from Refs. [45,46]. The EKM and EMN results correspond to the results shown in Fig. 2 of Ref. [9] for the differential cross section (of course with a different meaning of the bands) and give a reasonable, although not perfect, agreement with data. The experimental ratio is slightly overestimated at lower angles and somewhat underestimated for $\theta \geqslant 50^\circ$. The differences between the EKM and EMN results are small and not crucial, EKM gives a smaller cross section around the maxima and therefore a somewhat better agreement with the data in this region. The bands, representing the uncertainties on the regularization of the NN chiral potentials, are generally small and not influential for the comparison with data. The KD result gives a good description of the experimental cross section for $\theta \leqslant 20^\circ$ and underpredicts the data for larger angles. We point out, to be honest, that KD was obtained for nuclei in the mass range $24 \leqslant A \leqslant 209$ while ^{16}O is below this range. We present the result only for the sake of comparison.

The ratios of the differential cross section to the Rutherford cross section for elastic proton scattering off calcium, nickel, tin, and lead isotopes are shown in Figs. 2–5. The results are compared with the experimental data taken from Refs. [45,46].

All the results for ^{40,42,44,48}Ca isotopes in Fig. 2 are for an incident-proton energy of 200 MeV. The experimental database used to generate the KD potential includes ^{40}Ca at $E = 200$ MeV. In Fig. 2 KD gives indeed an excellent agreement with ^{40}Ca data, and a good agreement also for the other isotopes. The results with the EKM and EMN potentials are very close to each other, the uncertainty bands are narrow, and the agreement with data, which is reasonable and of about the same quality for all the isotopes, is however somewhat worse than with KD, in particular at larger angles. At lower angles the EKM and EMN results well reproduce the behavior of the experimental cross section, which is sometimes a bit overestimated by the calculations. A better agreement with data would presumably be obtained by improving or reducing the approximations adopted in the calculation of the microscopic OP.

In Fig. 3 we show the results for ^{58}Ni at $E = 192$ and 295 MeV, ^{60}Ni at $E = 178$ MeV, and ^{62}Ni at $E = 156$ MeV. The experimental database used to generate the KD potential includes ^{58}Ni up to 200 MeV and ^{60}Ni up to 65 MeV. For ^{58}Ni KD gives a good description of the data at 192 MeV, while a much worse agreement is obtained at the higher energy of 295 MeV, where only the overall behavior of the experimental cross section is reproduced by the phenomenological OP. The EKM and EMN results give a better and reasonable description of the data at 295 MeV, up to $\theta \sim 40^\circ$. At 192 MeV the microscopic OP can roughly describe the shape of the experimental cross section, but the size is somewhat overestimated. KD gives only a poor description of the data for ^{60}Ni at 178 MeV and a very good agreement for ^{62}Ni at 156 MeV. The microscopic OP gives a better and reasonable agreement with the ^{60}Ni data, over all the angular distribution, while for ^{62}Ni the results are a bit larger than those of the KD potential. The EKM and EMN results are always very close to each other and the bands are generally narrow.

The results for ^{116,118,120,122,124}Sn isotopes at 295 MeV and for ^{120}Sn at 200 MeV are displayed in Fig. 4. In this case all the OPs give qualitatively similar results and a reasonable agreement with data, in particular, for $\theta \leqslant 20^\circ$. The agreement generally declines for larger angles. KD gives a better description of ^{120}Sn data at 200 MeV, where the EKM and EMN results are a bit larger than the data at the maxima and a bit lower at the minima. We note that ^{120}Sn is included in the experimental database for the KD potential for proton energies up to 160 MeV. At 295 MeV, the microscopic OP gives, in general, a slightly better agreement with the data than KD for all the tin isotopes shown in the figure.

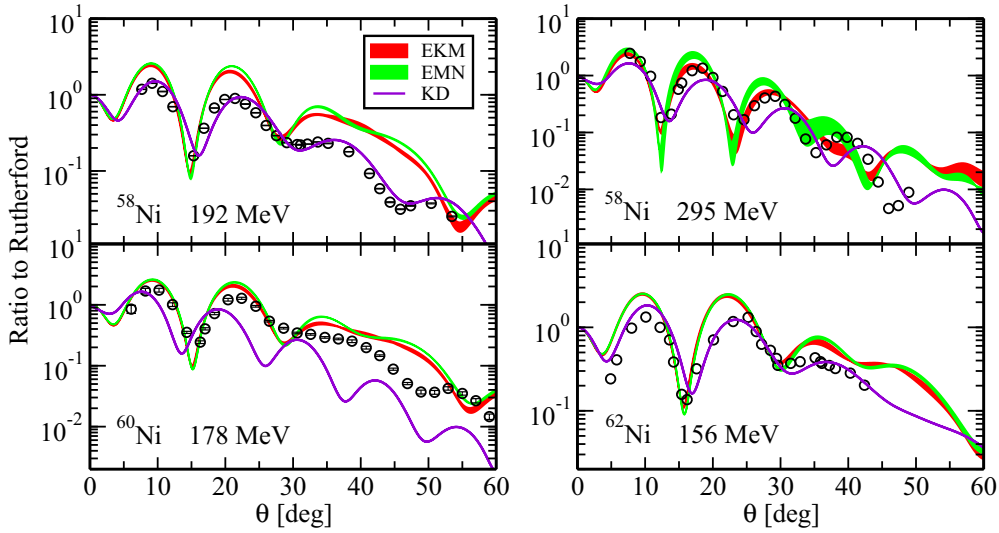

FIG. 3. The same as in Fig. 1 for Ni isotopes: ^{58}Ni at $E = 192$ and 295 MeV, ^{60}Ni at $E = 178$ MeV, and ^{62}Ni at $E = 156$ MeV. Experimental data are from Refs. [45,46].

The results for ^{204,206,208}Pb isotopes at 295 MeV and for ^{208}Pb data at 200 MeV are displayed in Fig. 5. Also in this case the experimental cross section at 200 MeV is well described by KD; the agreement is better than with the microscopic OP. The experimental database for KD includes ^{208}Pb up to 200 MeV. At 295 MeV a better agreement with data is generally given by the EKM and EMN results, in particular by EMN: for all three isotopes considered, the two results practically overlap for $\theta \leqslant 20^{\circ}$, where they are also very close to the KD result, then they start to separate and the EMN result is a bit larger than the EKM one and in better agreement with data. We point out that the uncertainty bands, which are generally narrow, in this case become larger and increase with the scattering angle, when also the agreement with data declines.

The results that we have shown until now indicate that, in comparison with the phenomenological KD potential, our

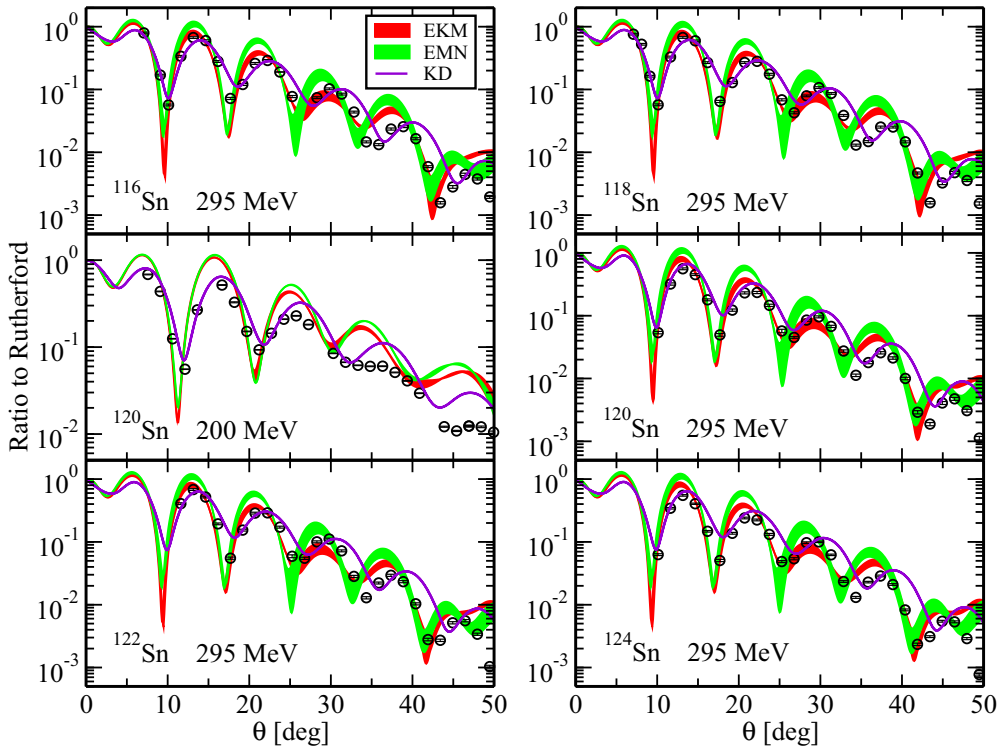

FIG. 4. The same as in Fig. 1 for Sn isotopes: ^{120}Sn at $E = 200$ MeV and ^{116,118,120,122,124}Sn at $E = 295$ MeV. Experimental data are from Refs. [45,46].

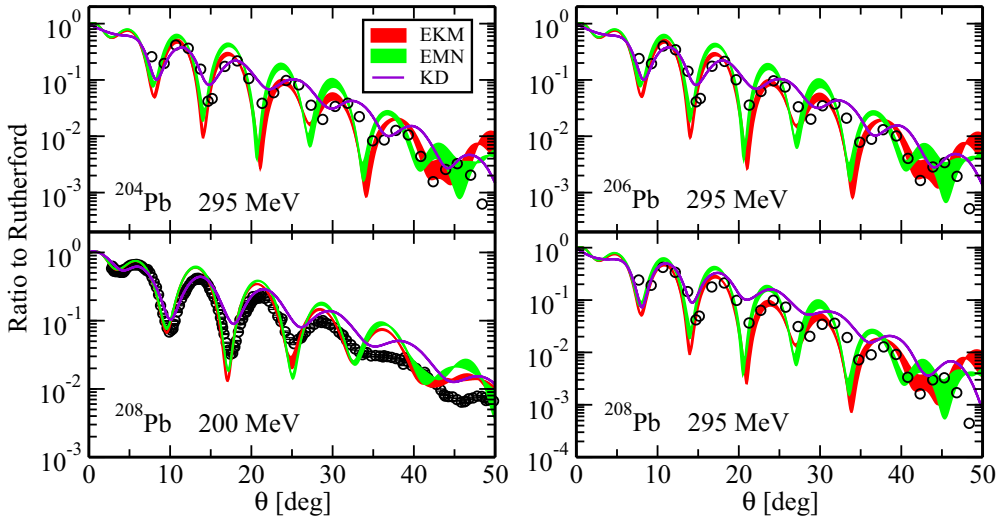

FIG. 5. The same as in Fig. 1 for Pb isotopes: ^{208}Pb at $E = 200$ MeV and ^{204,206,208}Pb at $E = 295$ MeV. Experimental data are from Refs. [45,46].

microscopic OP, in spite of the approximations made to derive it, has a comparable and in some cases even better predictive power in the description of the cross sections on the isotopic chains and energy range here considered. KD is able to give a better and excellent description of data in specific situations, in particular, for data included in the experimental database used to obtain the parameters of the phenomenological KD potential and at the lower energies considered. Our microscopic OP is able to give a similar and more homogeneous description of data for all the nuclei of an isotopic chain and, for energies above 200 MeV, it gives, in general, a better agreement with data than the phenomenological KD potential. This conclusion is confirmed by the results shown in Fig. 6, where the ratios of the differential cross section to the Rutherford cross section are displayed for elastic proton scattering off ^{16}O and ^{40,42,44,48}Ca at $E = 318$ MeV and ^{58}Ni at $E = 333$ MeV in comparison with the data taken from Refs. [45,46]. The differences between the results of the phenomenological

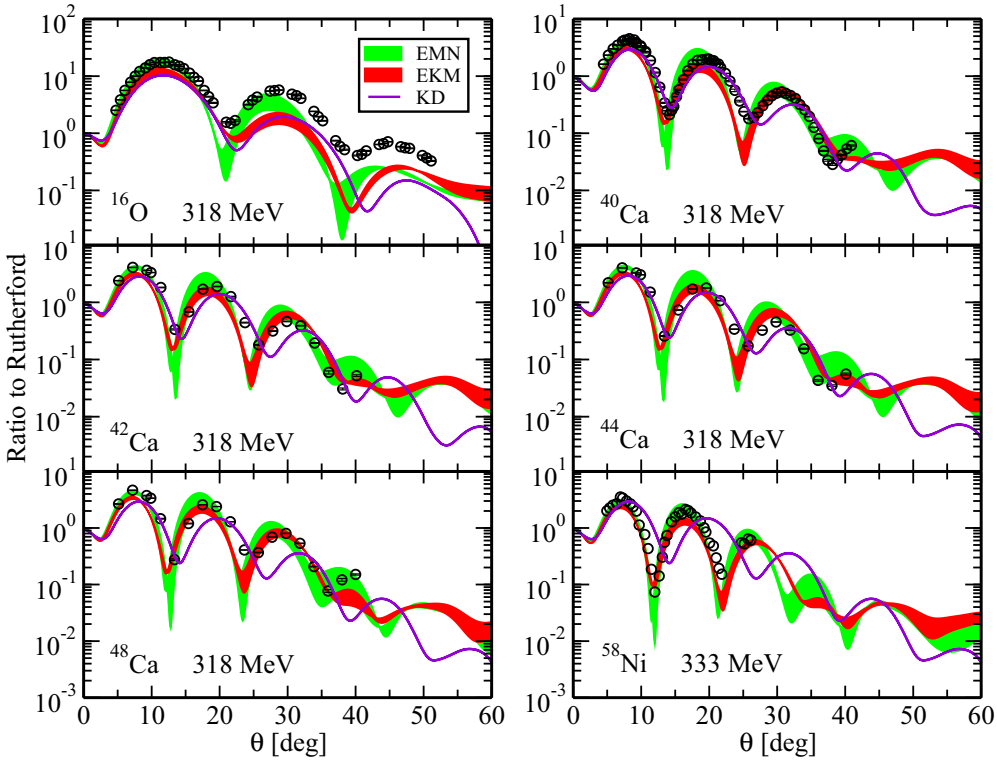

FIG. 6. The same as in Fig. 1 for ^{16}O and ^{40,42,44,48}Ca at $E = 318$ MeV and ^{58}Ni at $E = 333$ MeV. Experimental data are from Refs. [45,46].

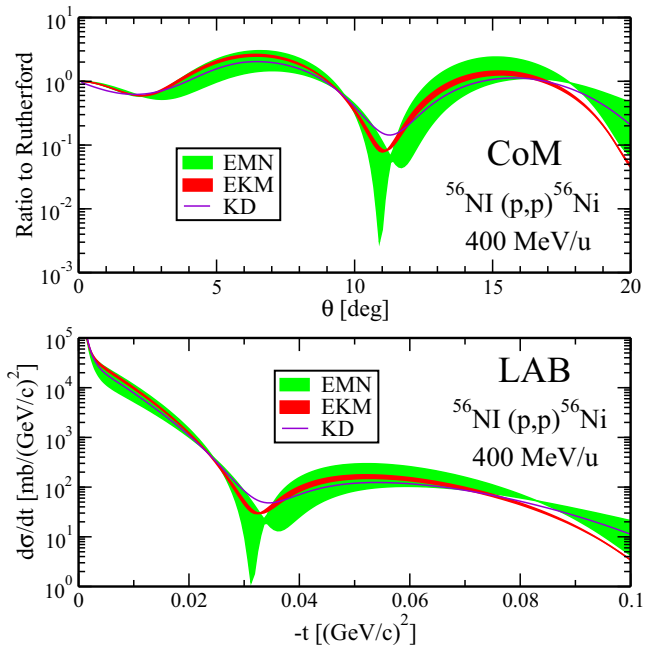

FIG. 7. (upper panel) Ratio of the differential cross section to the Rutherford cross section as a function of the center-of-mass scattering angle θ for ^{56}Ni(p, p)^{56}Ni elastic scattering at $E = 400$ MeV/u. (lower panel) Differential cross section as a function of the Mandelstam variable t in the laboratory frame for ^{56}Ni(p, p)^{56}Ni elastic scattering at $E = 400$ MeV/u. Calculations are performed with the microscopic OPs derived from the EKM [17,19] (EKM, red band) and EMN [20,21] (EMN, green band) NN chiral potentials at N^{4}LO and with the phenomenological global OP of Ref. [42] (KD, violet line). The interpretation of the bands is explained in the text and differs from that of Fig. 1.

and microscopic OPs increase with the increasing scattering angle and proton energy. For ^{58}Ni at 333 MeV both EKM and EMN give a much better and very good description of data. In the other cases KD is able to describe data only at the lowest angles. The EKM and EMN results are in general very close to each other. In both cases the width of the uncertainty bands increases at larger scattering angles but the uncertainties are not crucial for the comparison with data.

As mentioned in the Introduction (Sec. I), in the near future new experimental data will be available for exotic nuclei [3,4]. For this purpose, in Fig. 7 we show theoretical predictions for EKM and EMN potentials for the test case ^{56}Ni(p, p)^{56}Ni at an energy of 400 MeV/u. In the upper panel we display the results for the ratio of the differential cross section to the Rutherford cross section as a function of the center-of-mass scattering angle θ, while in the lower panel we display the differential cross section in the laboratory frame as a function of the Mandelstam variable t. Here the transformation of the differential cross section from the center of mass to the laboratory frame is done according to Chapter 2 of Ref. [47], while the transformation to the Mandelstam variable t is performed following Chapter 4 of Ref. [48]. Even if the energy scale involved is beyond the supposed range of validity of our approach, it is interesting to see if the results of the microscopic and KD potentials look reasonable and if error bands are acceptable. We only included a selection of the potentials because of the energy: $R = 0.8$ and 0.9 fm for EKM potentials and $\Lambda = 500$ and 550 MeV for the EMN ones. At 400 MeV/u, KD and EKM give similar predictions with reasonable shapes while the EMN potentials give a larger band compared with the EKM one and in the region of the minimum they produce two different minima, indicating that, at this energy, the potentials are not completely under control and they strongly depend on the choice of Λ. With the increasing scattering angle θ up to 60° the EMN band becomes larger and larger and, for $\theta > 30°$, the EMN potential is also not completely under control anymore. However, in Fig. 7 we show the results only for $\theta \leqslant 20°$, because, due to the challenges of inverse kinematics, the regime of the elastic scattering may be focused at small center-of-mass angles [5,49] corresponding to $t \approx -0.1$ (GeV/c)^2 in the laboratory system. Unfortunately, experimental data are

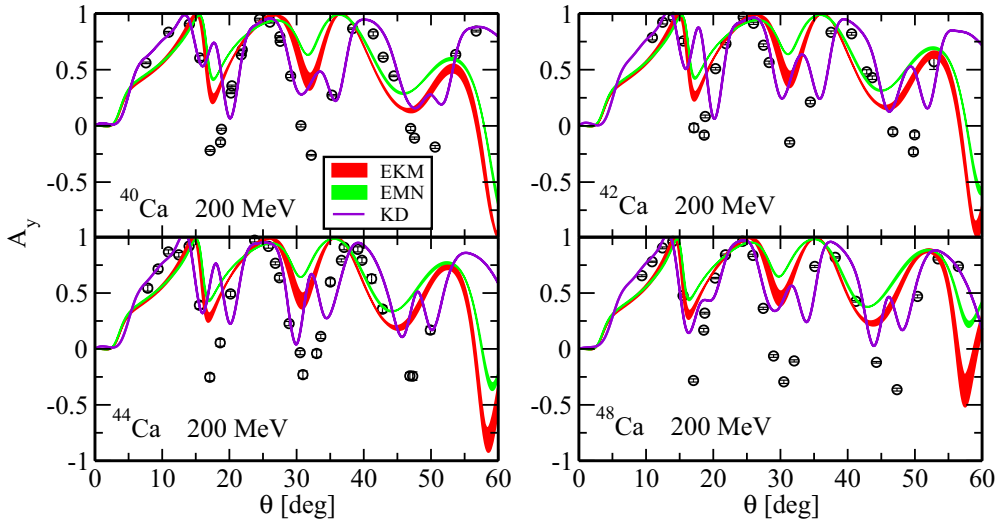

FIG. 8. The same as in Fig. 2 but for the analyzing power A_y. Experimental data are from Refs. [45,46].

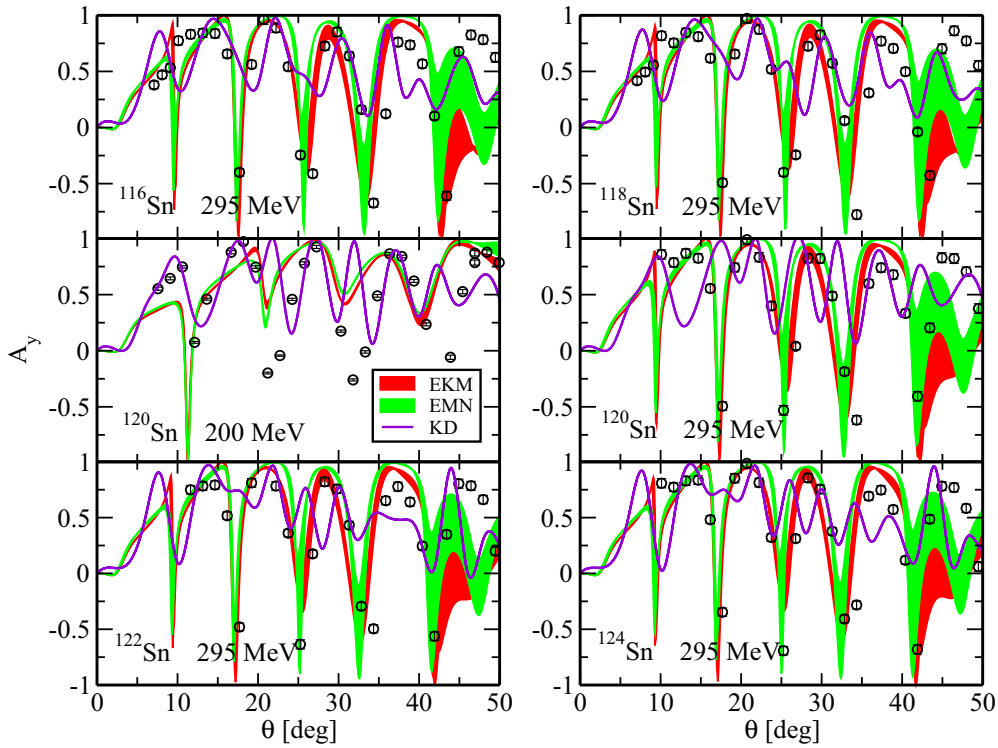

FIG. 9. The same as in Fig. 4 but for the analyzing power A_y. Experimental data are from Refs. [45,46].

still under scrutiny and not yet published [50]. From this figure we can thus conclude that, contrary to the EMN potentials, the EKM potentials have not yet reached the limit beyond which the chiral expansion scheme breaks down. Of course, this limit is not unique and depends on the regularization scheme adopted to derive the NN interaction.

In Figs. 8–10 we show the analyzing power A_y for some of the same nuclei and at the same proton energies presented in Figs. 1–5.

The analyzing power for calcium isotopes is shown Fig. 8, which corresponds to Fig. 2 for the ratio of the differential cross section to the Rutherford cross section. Polarization observables are usually more difficult to reproduce and also in this case the agreement with data is far from perfect, but all the results are able to describe the overall behavior of the experimental A_y, in particular at lower angles. A better result in comparison with data is given in this case by the phenomenological KD potential. The differences between the

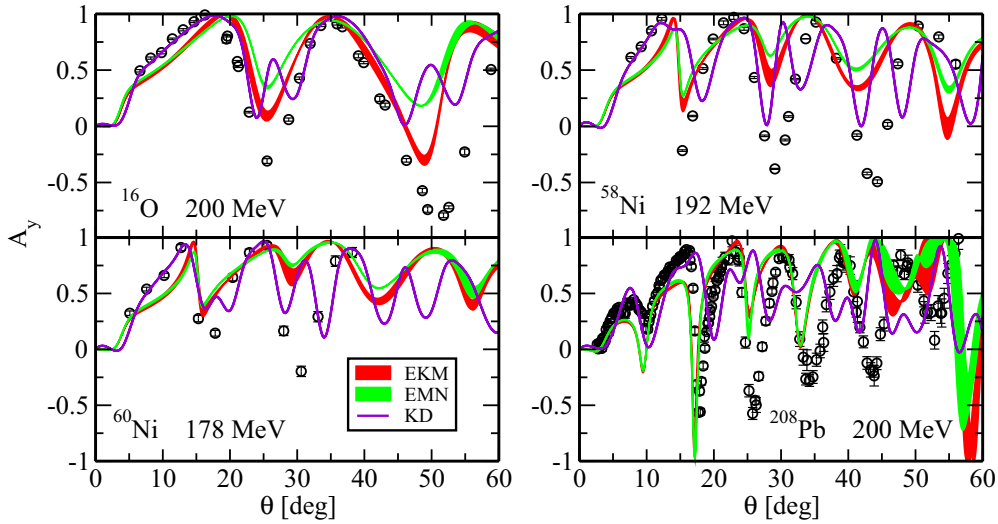

FIG. 10. Analyzing power A_y as a function of the angle θ for elastic proton scattering on ^{16}O, and ^{208}Pb at $E = 200$ MeV, ^{58}Ni at $E = 192$ MeV, and ^{60}Ni at $E = 178$ MeV. Experimental data are from Refs. [45,46].

EKM and EMN results are small, but the error bands get large at the largest angles considered.

The results for tin isotopes in Fig. 9 correspond to the results of Fig. 4 for the ratio $\frac{d\sigma}{d\Omega}/\frac{d\sigma}{d\Omega}_{\rm Ruth}$. Also in this case the agreement with data is worse than in Fig. 4 and it is difficult to judge which OP gives the better description of the experimental A_y: KD is somewhat better at 200 MeV and the microscopic OP at 295 MeV. It must be emphasized that the extension to 1 GeV was performed to have the total reaction cross section under control up to this energy with no concerns about polarization observables. The bad performance in the description of A_y is anyhow not surprising if we consider that Woods–Saxon-like form factors are not supposed to work properly above 200 MeV [51].

The analyzing power for ^{16}O and ^{208}Pb at 200 MeV, ^{58}Ni at 192 MeV, and ^{60}Ni at 178 MeV are displayed in Fig. 10. In the case of ^{16}O, the results basically confirm what was already found for the ratio in Fig. 1: KD gives a good description of data for lower angles, in particular for $\theta \leqslant 20^\circ$, EKM and EMN give a less good description of data at lower angles but a reasonable agreement up to $\theta \sim 50^\circ$. The experimental analyzing powers of ^{58}Ni and ^{60}Ni are well described by KD at the lowest angles but, overall, for the angular distribution the general agreement (or disagreement) with data of the microscopic and phenomenological OPs is of about the same quality. Also in the case of ^{208}Pb KD describes the experimental A_y well for $\theta \leqslant 20^\circ$, better than the EKM and EMN results, which, on the other hand, are in a somewhat better (although not perfect) agreement with data for larger angles.

IV. CONCLUSIONS

In recent papers [8,9] we derived a microscopic optical potential for elastic pA scattering from NN chiral potentials at fourth order (N^3LO) and fifth order (N^4LO), with the purpose to study the domain of applicability of NN chiral potentials to the construction of an optical potential, to investigate convergence patterns, and to assess the theoretical errors associated with the truncation of the chiral expansion. Numerical examples for the cross section and polarization observables of elastic proton scattering off ^{12}C, ^{16}O, and ^{40}Ca nuclei were presented and compared with available experimental data. Our results indicated that building an optical potential within the chiral perturbation theory is a promising approach for describing elastic proton-nucleus scattering and they allowed us to conclude that convergence has satisfactorily been achieved at N^4LO.

In the present work we have extended our previous investigation to isotopic chains exploring the mass number dependence and the energy range of applicability of our microscopic optical potential. As a benchmark, we have tested our calculations against one of the best phenomenological parametrizations developed by Koning and Delaroche [10] and, of course, experimental data where available.

Our main goal was to check the robustness of our approach and the capability of our optical potential to be applied to exotic nuclei, i.e., nuclei with values of proton-to-neutron ratio far from the stability, where phenomenological models might be unreliable.

Numerical results have been presented for the unpolarized differential cross section and the analyzing power of elastic proton scattering off calcium, nickel, tin, and lead isotopes in a proton energy range between 156 and 333 MeV. A theoretical prediction for the cross section of elastic proton scattering off ^{56}Ni at 400 MeV has also been presented, which is of interest for the future EXL experiment on exotic nuclei at FAIR [3,4], although the energy is beyond the supposed range of validity of the chiral potentials.

Because of the renormalization procedure, NN chiral potentials with almost the same level of accuracy (i.e., the χ^2 associated with the reproduction of NN phase shifts) come with different values of the cutoff parameters. We have restricted our calculations to a limited set of the aforementioned parameters and we have associated theoretical error bands to the uncertainties produced by the different parameters.

The agreement of our present results with empirical data is sometimes worse and sometimes better but overall comparable to the agreement given by the phenomenological OP, in particular for energies close to 200 MeV and above 200 MeV. The example shown at 400 MeV suggests that, at this energy, the EKM potentials have not yet reached the limit after which the chiral expansion scheme breaks down.

The microscopic optical potential generally provides a qualitatively similar agreement with data for all the nuclei of an isotopic chain. This clearly shows that changing the values of A does not affect the predictive power of our optical potential. The agreement is worse for the analyzing power than for the cross section and in general declines for larger values of the scattering angle.

Our theoretical predictions can be improved as suggested by some recent works. In particular we would like to mention three possible extensions on which we plan to work in the near future. We believe that the main improvement, at least from the theoretical side, would be the inclusion of three-body forces in the nuclear potential. An exact treatment is of course not possible for our purposes but, as suggested by many authors [52–55], it is possible to include three-body forces as an effective two-body density-dependent force where the third nuclear degree of freedom is basically averaged over the nucleon Fermi sphere. Even if in Ref. [54] the authors claim that the inclusion of three-body forces has a small impact on cross sections, the importance on analyzing powers or spin rotations could be larger.

The second improvement would be to consider medium effects because, at the moment, we describe nucleons with unperturbed Green's functions (see page 3 of Ref. [8]). In the past Elster *et al.* [31–33] introduced mean-field potentials in the definition of the single-particle propagator while, more recently, Barbieri *et al.* [56] used the self-consistent Green's function theory to produce *ab initio* optical potentials. The authors claim that, at least for low energies, it is possible to reproduce scattering observables in medium-mass nuclei from first principles. With the ambition to perform full *ab initio* calculations we will explore in a future paper the possibility

of including in our framework realistic *ab initio* Green's functions built upon chiral forces.

Finally, the third improvement consists of going beyond the optimum factorization and calculating the full-folding integral. This has already been done for light nuclei in Ref. [40], where nonlocal *ab initio* densities have been derived within the NCSM [41] approach. Unfortunately, due to the expensive computational task, it is possible to perform such calculations only up to *sd*-shell nuclei. An alternative approach has been proposed in Ref. [57] where the Green's function approach is combined to the coupled-cluster method [58,59] to compute the optical potential.

ACKNOWLEDGMENTS

The authors are deeply grateful to E. Epelbaum (Institut für Theoretische Physik II, Ruhr–Universität Bochum, Germany) for providing the chiral potential of Refs. [17,19] and R. Machleidt (Department of Physics, University of Moscow, Idaho, USA) for the chiral potential of Refs. [20,21]. We also would like to acknowledge useful communications with A. Koning (Nuclear Research and Consultancy Group NRG, Petten, The Netherlands) and T. Kröll (Institut für Kernphysik, Technische Universität Darmstadt, Germany). TRIUMF receives federal funding via a contribution agreement with the National Research Council of Canada.

[1] H. Paetz gen. Schieck, *Nuclear Reactions* (Springer-Verlag, Berlin, Heidelberg, 2014).
[2] N. K. Glendenning, *Direct Nuclear Reactions* (World Scientific Press, Singapore, 2004).
[3] https://www.gsi.de/work/forschung/nustarenna/nustarfair.htm.
[4] https://www.rug.nl/kvi-cart/research/hnp/research/exl/.
[5] M. von Schmid, S. Bagchi, S. Bönig, M. Csatlós, I Dillmann, C. Dimopoulou, P. Egelhof, V. Eremin, T. Furuno, H. Geissel, R. Gernhäuser, M. N. Harakeh, A.-L. Hartig, S. Ilieva, N. Kalantar-Nayestanaki, O. Kiselev, H. Kollmus, C. Kozhuharov, A. Krasznahorkay, T. Kröll, M. Kuilman, S. Litvinov, Yu A. Litvinov, M. Mahjour-Shafiei, M. Mutterer, D. Nagae, M. A. Najafi, C. Nociforo, F. Nolden, U. Popp, C. Rigollet, S. Roy, C. Scheidenberger, M. Steck, B. Streicher, L. Stuhl, M. Thürauf, T. Uesaka, H. Weick, J. S. Winfield, D. Winters, P. J. Woods, T. Yamaguchi, K. Yue, J. C. Zamora, and J. Zenihiro, EPJ Web Conf. **66**, 03093 (2014).
[6] H. Feshbach, Ann. Phys. (NY) **5**, 357 (1958).
[7] W. H. Dickhoff, R. J. Charity, and M. H. Mahzoon, J. Phys. G **44**, 033001 (2017).
[8] M. Vorabbi, P. Finelli, and C. Giusti, Phys. Rev. C **93**, 034619 (2016).
[9] M. Vorabbi, P. Finelli, and C. Giusti, Phys. Rev. C **96**, 044001 (2017).
[10] A. J. Koning and J. P. Delaroche, Nucl. Phys. A **713**, 231 (2003).
[11] A. Koning, D. Rochman, and S. van der Marck, Nucl. Data Sheets **118**, 187 (2014).
[12] J. P. Jeukenne, A. Lejeune, and C. Mahaux, Phys. Rep. **25**, 83 (1976).
[13] C. Mahaux, P. F. Bortignon, R. A. Broglia, and C. H. Dasso, Phys. Rep. **120**, 1 (1985).
[14] R. Machleidt, Adv. Nucl. Phys. **19**, 189 (1989).
[15] R. Machleidt and D. R. Entem, Phys. Rep. **503**, 1 (2011).
[16] E. Epelbaum, H.-W. Hammer, and U.-G. Meißner, Rev. Mod. Phys. **81**, 1773 (2009).
[17] E. Epelbaum, H. Krebs, and U.-G. Meißner, Eur. Phys. J. A **51**, 53 (2015).
[18] R. L. Varner, W. J. Thompson, T. L. McAbee, E. J. Ludwig, and T. B. Clegg, Phys. Rep. **201**, 57 (1991).
[19] E. Epelbaum, H. Krebs, and U.-G. Meißner, Phys. Rev. Lett. **115**, 122301 (2015).
[20] D. R. Entem, N. Kaiser, R. Machleidt, and Y. Nosyk, Phys. Rev. C **91**, 014002 (2015).
[21] D. R. Entem, R. Machleidt, and Y. Nosyk, Phys. Rev. C **96**, 024004 (2017).
[22] W. B. Riesenfeld and K. M. Watson, Phys. Rev. **102**, 1157 (1956).
[23] A. K. Kerman, H. McManus, and R. M. Thaler, Ann. Phys. (NY) **8**, 551 (1959).
[24] A. Picklesimer, P. C. Tandy, R. M. Thaler, and D. H. Wolfe, Phys. Rev. C **30**, 1861 (1984).
[25] C. Elster and P. C. Tandy, Phys. Rev. C **40**, 881 (1989).
[26] C. Elster, T. Cheon, E. F. Redish, and P. C. Tandy, Phys. Rev. C **41**, 814 (1990).
[27] H. F. Arellano, F. A. Brieva, and W. G. Love, Phys. Rev. Lett. **63**, 605 (1989).
[28] H. F. Arellano, F. A. Brieva, and W. G. Love, Phys. Rev. C **41**, 2188 (1990).
[29] R. Crespo, R. C. Johnson, and J. A. Tostevin, Phys. Rev. C **41**, 2257 (1990).
[30] R. Crespo, R. C. Johnson, and J. A. Tostevin, Phys. Rev. C **46**, 279 (1992).
[31] C. R. Chinn, C. Elster, and R. M. Thaler, Phys. Rev. C **48**, 2956 (1993).
[32] C. R. Chinn, C. Elster, R. M. Thaler, and S. P. Weppner, Phys. Rev. C **51**, 1418 (1995).
[33] C. R. Chinn, C. Elster, R. M. Thaler, and S. P. Weppner, Phys. Rev. C **52**, 1992 (1995).
[34] C. Elster, S. P. Weppner, and C. R. Chinn, Phys. Rev. C **56**, 2080 (1997).
[35] K. Amos, P. J. Dortmans, H. V. von Geramb, S. Karataglidis, and J. Raynnal, *Nucleon-Nucleus Scattering: A Microscopic Nonrelativistic Approach*, in *Advances in Nuclear Physics*, edited by J. W. Negele and E. Vogt (Springer US, Boston, 2002), pp. 276–536.
[36] H. F. Arellano, F. A. Brieva, and W. G. Love, Phys. Rev. C **52**, 301 (1995).
[37] H. F. Arellano and E. Bauge, Phys. Rev. C **84**, 034606 (2011).
[38] T. Nikšić, N. Paar, D. Vretenar, and P. Ring, Comput. Phys. Commun. **185**, 1808 (2014).
[39] T. Nikšić, D. Vretenar, P. Finelli, and P. Ring, Phys. Rev. C **66**, 024306 (2002).
[40] M. Gennari, M. Vorabbi, A. Calci, and P. Navratil, Phys. Rev. C **97**, 034619 (2018).
[41] B. R. Barrett, P. Navrátil, and J. P. Vary, Prog. Part. Nucl. Phys. **69**, 131 (2013).
[42] A. J. Koning, S. Hilaire, and M. C. Duijvestijn, *Proceedings of the International Conference on Nuclear Data for Science and Technology, April 22–27, 2007, Nice, France* (2008), p. 211.
[43] J. Raynal, Notes on ecis94, Note CEA-N-2772 (1994).
[44] www.talys.eu/fileadmin/talys/user/docs/talys1.8.pdf.

[45] http://www.physics.umd.edu/enp/jjkelly/datatables.htm.
[46] http://www.nndc.bnl.gov/exfor/exfor.htm.
[47] C. Joachain, *Quantum Collision Theory* (North-Holland, Amsterdam, 1975).
[48] E. Byckling and K. Kajantie, *Particle Kinematics* (Wiley, London, 1973).
[49] P. Egelhof, S. Bagchi, S. Bönig, M. Csatlós, I. Dillmann, C. Dimopoulou, V. Eremin, T. Furuno, H. Geissel, R. Gernhäuser, M. N. Harakeh, A.-L. Hartig, S. Ilieva, N. Kalantar-Nayestanaki, O. Kiselev, H. Kollmus, C. Kozhuharov, A. Krasznahorkay, T. Kröll, M. Kuilman, S. Litvinov, Y. A. Litvinov, M. Mahjour-Shafiei, M. Mutterer, D. Nagae, M. A. Najafi, C. Nociforo, F. Nolden, U. Popp, C. Rigollet, S. Roy, C. Scheidenberger, M. V. Schmid, M. Steck, B. Streicher, L. Stuhl, M. Thürauf, T. Uesaka, H. Weick, J. S. Winfield, D. Winters, P. J. Woods, T. Yamaguchi, K. Yue, J. C. Zamora, and J. Zenihiro, in Proceedings of the Conference on Advances in Radioactive Isotope Science (ARIS2014), JPS Conf. Proc. **6**, 020049 (2015).
[50] T. Kröll (private communication).
[51] A. J. Koning (private communication); an improvement could be obtained by adjusting some parameters in TALYS (i.e., v4adjust, w3adjust, or w4adjust).
[52] J. W. Holt, N. Kaiser, and W. Weise, Phys. Rev. C **81**, 024002 (2010).
[53] M. Kohno, Phys. Rev. C **88**, 064005 (2013).
[54] M. Toyokawa, M. Yahiro, T. Matsumoto, K. Minomo, K. Ogata, and M. Kohno, Phys. Rev. C **92**, 024618 (2015).
[55] J. W. Holt, N. Kaiser, and G. A. Miller, Phys. Rev. C **93**, 064603 (2016).
[56] A. Idini, C. Barbieri, and P. Navrátil, Acta Phys. Pol., B **48**, 273 (2017).
[57] J. Rotureau, P. Danielewicz, G. Hagen, F. M. Nunes, and T. Papenbrock, Phys. Rev. C **95**, 024315 (2017).
[58] G. Hagen, T. Papenbrock, M. Hjorth-Jensen, and D. J. Dean, Rep. Prog. Phys. **77**, 096302 (2014).
[59] R. J. Bartlett and M. Musiał, Rev. Mod. Phys. **79**, 291 (2007).